IOPscience iopscience.iop.org

Home Search Collections Journals About Contact us My IOPscience

Stable zipping RF MEMS varactors

This article has been downloaded from IOPscience. Please scroll down to see the full text article.

2010 J. Micromech. Microeng. 20 035030

(http://iopscience.iop.org/0960-1317/20/3/035030)

The Table of Contents and more related content is available

Download details:
IP Address: 155.198.134.118
The article was downloaded on 13/04/2010 at 14:03

Please note that terms and conditions apply.

J. Micromech. Microeng. **20** (2010) 035030 (8pp) doi:10.1088/0960-1317/20/3/035030

Stable zipping RF MEMS varactors

Suan Hui Pu, Andrew S Holmes, Eric M Yeatman, Christos Papavassiliou and Stepan Lucyszyn

Department of Electrical and Electronic Engineering, Imperial College London, London SW7 2AZ, UK

E-mail: suanhui.pu02@imperial.ac.uk

Received 25 August 2009, in final form 22 January 2010
Published 2 March 2010
Online at stacks.iop.org/JMM/20/035030

Abstract
Novel zipper varactors with the potential for achieving large tuning ranges have been fabricated and characterized. These varactors have a curved cantilever electrode that is actuated by a single pull-down electrode. The shape of the cantilever is designed such that its local stiffness is tailored to enable extended stable zipping. In a series-mounted varactor, the measured capacitance ratio was 16.5 for actuation voltages between 0 and 46 V. However, the presence of an unexpected tuning instability at 32 V bias limited the practical tuning range in this varactor. This behaviour was attributed to fabrication imperfections. The first electrical self-resonant frequency of the same varactor was extrapolated to be 72.6 and 17.2 GHz at 20 and 329 fF, respectively. In a different shunt-mounted varactor, the quality factor (Q) was measured to be 91 (60 fF) and 176 (600 fF) at 2 GHz. Including the anchor, the varactors have a small device footprint and fit within an area of 500 by 100 μm.

(Some figures in this article are in colour only in the electronic version)

1. Introduction

In reconfigurable radio frequency (RF) systems, varactors with low loss and a large continuous tuning range (TR) are of key importance. Recently, varactors implemented using microelectromechanical system (MEMS) technology have emerged as viable alternatives to semiconductor varactors due to their high quality (Q) factors and superior tunability [1, 2]. Very large TRs (>3000%) have been demonstrated in MEMS varactors [3–5], along with high Q-factor values of up to 500 at microwave frequencies [4–7]. The tuning range of a varactor is defined as $\mathrm{TR} = (C_2 - C_1)/C_1 \times 100\%$, where the device capacitance can be tuned continuously between C_1 and C_2 ($C_2 > C_1$). While it is possible to achieve good TRs with solid-state varactors (>500%), their Q-factor values remain in the region of around 20. Hence, despite having drawbacks such as slower tuning speeds and shorter operating lifetimes, RF MEMS varactors are good candidates for implementing low-loss tunable systems.

MEMS varactors are typically tuned either by varying the gap distance between the capacitor electrodes [3, 4, 7, 8] or by changing their electrode overlap area [5, 9]. The majority of these varactors employ electrostatic actuation due to its ease of implementation and low-power consumption. However, electrostatically gap-tuned designs consisting of a parallel plate suspended by linear springs suffer from pull-in instability, limiting the TR to 50% or less [10]. In order to overcome this limitation, dual-gap designs have been implemented where independent actuation electrodes are incorporated for varactor tuning [4, 7, 11, 12]. By designing the capacitor gap to be smaller than a third of the actuator gap, the device tunability can be extended substantially [4]. Gap-tuned varactors using other methods of actuation (e.g. piezoelectric or thermal) have also been proposed, avoiding the electrostatic pull-in instability. However, their disadvantages include increased device complexity, along with slower actuation and higher power consumption for the thermally actuated varactors [3, 13, 14].

Area-tuned RF MEMS varactors usually consist of laterally actuated interdigital comb fingers where the movable parts are connected to flexible suspensions. Highly controllable capacitance–voltage (C–V) responses along with good tunability have been demonstrated using this approach [9, 15]. In order to avoid the use of long, compliant suspensions, a comb-drive varactor utilizing angular motion to vary its area of overlap has been reported, yielding a TR of more than 3000% [5].

In this work, a new RF MEMS zipping varactor with a large tuning range is presented. Stable zipping varactors were first demonstrated by Hung and Senturia [16]. These varactors consist of a straight polysilicon cantilever which is pulled down towards the bottom electrode by applying a bias

 © 2010 IOP Publishing Ltd Printed in the UK

voltage greater than the pull-in voltage. Upon contact, the movable electrode behaves like a 'fixed-fixed' beam, and zips in an 'S-shaped' configuration towards the beam anchor. Due to mechanical nonlinearity, the bottom electrode shape of the device was optimized to provide a linear *C*–*V* characteristic. A linear TR of 25% (77% total TR) was achieved, although no RF measurements were reported as the prototypes were designed as proof-of-concept devices. Subsequent varactors of similar design have been reported by others [17–19]. Zipping varactors with curved cantilevers operating in a 'fixed-free' configuration have also been fabricated. Muldavin *et al* reported an analogue zipping varactor with two pull-down electrodes [20]. A capacitance ratio (i.e. the maximum capacitance divided by the minimum capacitance) of 32 was measured along with a useful working TR of 600%. However, due to modulation artefacts introduced by the bipolar control voltage, the authors subsequently adopted a multi-bit topology to implement varactors using capacitive switches.

Varactors that incorporate an electrode beam that zips in contact with a dielectric are particularly useful for implementing compact devices with large TRs. In particular, if the permittivity of the dielectric is high, the capacitance can be tuned from a very low value (when much of the air gap persists) to a very large value (when the air gap zips to closure). Such varactors will be useful either individually or when connected in parallel to extend the TR even further [21, 22]. In this paper we report on a zipping varactor which extends previous work, by incorporating a tapered zipping cantilever. This approach allows both mechanical and electrostatic characteristics to be tailored, allowing a large TR. A new fabrication approach is also presented which is well adapted for rapid prototyping.

2. Varactor design

The zipping varactor design consists of a curved cantilever electrode and a fixed bottom electrode that is covered by a thin insulating dielectric (see figure 1). Both the top and bottom electrodes are made of gold in order to minimize the series resistance of the device. To obtain the curvature in the cantilever, a thin layer with residual tensile stress is sputtered as the top layer of the cantilever while the thicker gold layer is relatively stress-free. The initial vertical displacement along the axis of the cantilever can be determined from plate theory as follows [23]:

$$v(x) = \frac{\sigma_2}{2(\tilde{E}_1 I_1' + \tilde{E}_2 I_2')}\left(h_2 d_2 - \frac{h_2^2}{2}\right) x^2 \qquad (1)$$

for $0 < x < L$. Subscripts 1 and 2 refer to parameters for the bottom (Au) and top (Cr/Cu) layers of the composite cantilever, respectively. σ_2 is the residual tensile stress and $\tilde{E}$ is the biaxial modulus, defined as $\tilde{E} = E/(1-\nu)$. E, ν and I' are Young's modulus, Poisson's ratio and the second moment of area (per unit width) about the composite cantilever's neutral axis. d_2 is the distance from the cantilever's top surface to its neutral axis and h_2 is the thickness of the top layer. This expression is valid for small deflections where the radius of curvature is much greater than the electrode thickness.

For controllable capacitance tuning, the curved cantilever of the zipping varactor is shaped such that its width increases linearly towards the free end [24]. This has the effect of increasing the *local stiffness* of the cantilever along its length from the anchor towards the free end. When a bias voltage is applied, the region near the anchor first comes into contact with the dielectric. The capacitance is then tuned by increasing the bias voltage and allowing the cantilever to zip onto the dielectric surface. Conversely, if both the fixed and movable electrodes are of constant width, then the device will have a switch characteristic due to the pull-in instability [25].

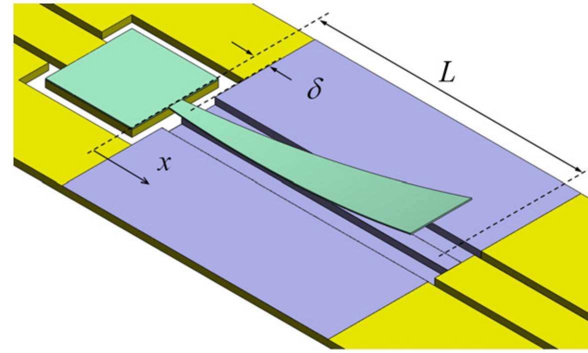

Figure 1. Illustration of a zipping varactor.

The analogue varactor of [20] uses two pull-down electrodes to tune the device over its entire TR. In contrast, the device reported here adopts a simple design with fewer device layers and only one actuating electrode. The varactor in [16] employs a different zipping concept where a straight cantilever is first pulled down into an 'S-shaped' configuration and then tuned by increasing the bias further. Since it is inherently stable after pull-in, it would have been possible to obtain stable zipping without electrode shaping. Nevertheless, to achieve a linear *C*–*V* response, the bottom electrode of the device was shaped to increase the *local electrostatic force* towards the anchor because of the stiffening effect of zipping. In our varactor, we retain the flexibility to tailor the shape of the bottom electrode in addition to the tailoring the shape of the cantilever. Gray *et al* demonstrated zipping actuators where the stiffness of the movable electrode was tailored to some degree [26, 27]. However, their devices were designed to be actuators with extended travel range rather than varactors [27]. As such, no RF measurements were reported although some dc capacitance measurements were performed.

The electromechanical behaviour of the new zipping varactor has been modelled in Coventor in order to predict device behaviour. Figure 2 shows the *C*–*V* characteristic for a zipping varactor with a cantilever length of 400 μm and an initial end height of approximately 46 μm. The bottom electrode width, b_e, is 20 μm and the cantilever width is given by the linear function $b(x) = 0.18x + 20$ μm for $0 < x < L$. The SiO_2 dielectric in the model is specified with a relative permittivity of 4 (ε_r), and a thickness of 0.23 μm (t_d). Table 1 provides a summary of the varactor parameters.

Between 0 and 10 V, the cantilever deflects downwards slightly with a 31% increase in capacitance (32–42 fF). At 10.5 V there is instability in the varactor, and a jump in capacitance occurs as the cantilever first comes into contact with the dielectric. Thereafter, the device operates in the

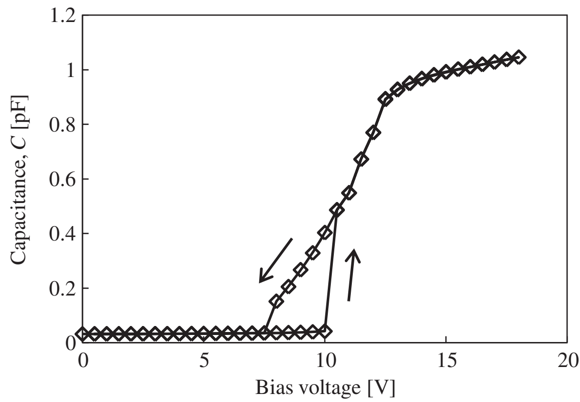

Figure 2. Predicted capacitance tuning in the Coventor model.

Table 1. Device parameters.

Parameter	Value	Parameter	Value
L	400 μm	h_1	1.1 μm
$b(x)$	$0.18x + 20$ μm	h_2	0.2 μm
b_e	20 μm	E_1	80 GPa
δ	20 μm	E_2	123 GPa
ε_r	4	ν_1	0.42
t_d	0.23 μm	ν_2	0.35
σ_2	150 MPa		

stable zipping mode. As the contact area of the cantilever and the dielectric increases, the varactor capacitance increases in a continuous manner. Beyond 13 V, the capacitance continues to increase but with a much smaller gradient. This is mainly due to additional zipping in the transverse direction as the curvature of the cantilever is biaxial in nature. When decreasing the bias voltage, it is observed that there is no hysteresis in the stable zipping region and the C–V characteristic is approximately linear between 13 and 8 V. For voltages up to 18 V, the continuous tuning obtained when increasing the bias voltage is between 0.49 and 1.05 pF (from 10.5–18 V). When decreasing the bias voltage, a larger continuous tuning of 1.05–0.15 pF (from 18 to 8 V) is obtained.

Figure 3 shows the degree of zipping in the varactor model at three bias voltage levels. Using the plate theory equation, the maximum displacement at zero bias is 44 μm, which agrees well with the finite element solution (46 μm). The

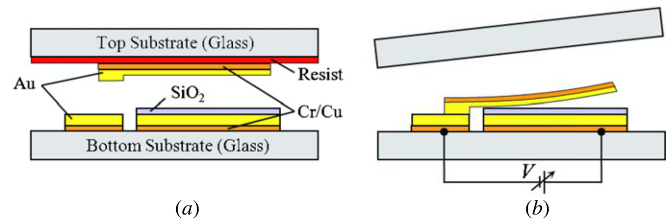

Figure 4. Fabrication and assembly showing (*a*) alignment of top and bottom parts; (*b*) bonding and release.

first mechanical resonant mode of this device (at 0 V bias) is obtained from the finite element model to be 1.95 kHz and the corresponding mechanical Q-factor is 5.7 in air under standard temperature and pressure conditions.

3. Fabrication

Zipping varactor prototypes have been fabricated using a four-mask process on two separate wafers. The fixed bottom electrode, CPW transmission lines and dielectric are patterned on a *bottom* wafer, while the cantilever is patterned on a *top* wafer with a release layer. A final die-level bonding step is used to complete the varactor assembly. This method of varactor fabrication was adopted to allow the flexibility of integrating a range of different dielectrics requiring very distinct deposition and patterning processes. Regardless of the bottom features, the same process for the curved cantilever can be adopted. Although a decrease in yield is inevitable in the assembly process, splitting the process across two wafers simplifies the process for each wafer and decreases development time. In the long term, a monolithic process can be developed for integration with a specific application circuit.

Figure 4 summarizes the varactor fabrication and assembly process. For the bottom wafer, a Cr/Cu seed layer (20 nm and 190 nm, respectively) is first sputtered onto a glass wafer. A layer of positive photoresist is then patterned to define a plating mould for the CPW line and bottom electrode. Subsequently, the wafer is plated with 60 nm of Ni and 3.1 μm of Au. Ni acts as a barrier to prevent Au–Cu interdiffusion which can result in reduced device reliability. Following resist removal and seed layer etch, 230 nm of SiO_2 is sputtered onto the wafer. This is then patterned by reactive ion etching (RIE) in a CHF_3/Ar plasma using a resist mask.

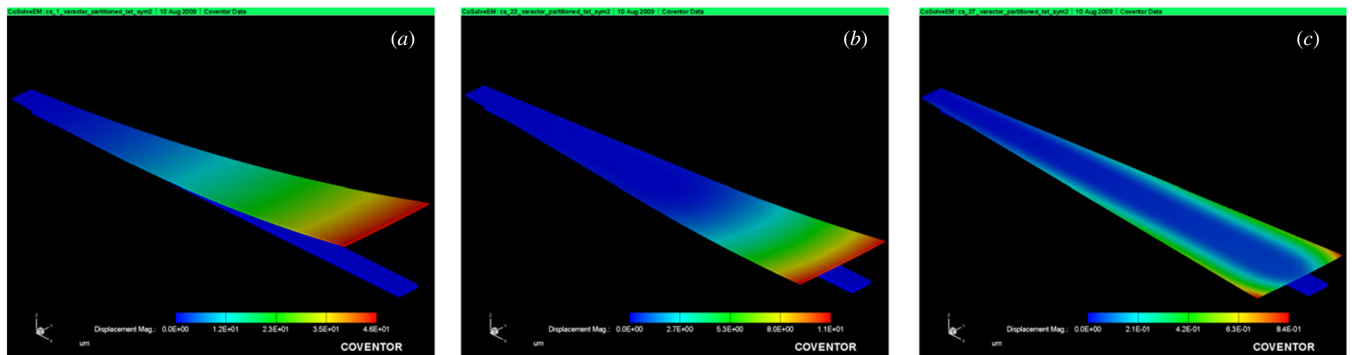

Figure 3. Model cantilever shape at different bias levels: (*a*) 0 V; (*b*) 11 V; and (*c*) 18 V.

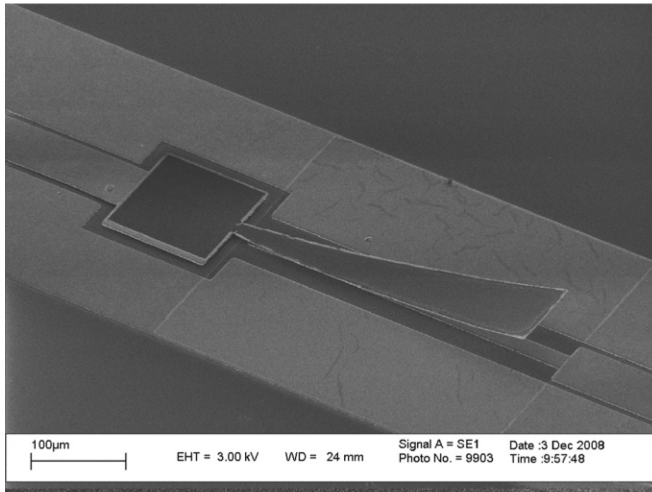

Figure 5. A series-mounted zipping varactor.

For the top wafer, a glass substrate with a thin layer of sacrificial resist is first sputtered with a Cr/Cu seed layer (50 nm and 150 nm, respectively). By adjusting the deposition parameters, the sputtered film obtains a residual tensile stress. A resist layer is then deposited and patterned to define the shape of the cantilever. Using the resist as a plating mould, the wafer is plated with 60 nm of Ni and 1.1 μm of gold. The anchor region is subsequently plated with an additional 0.5 μm of gold, and finally, the seed layer is etched using the electroplated layers as a mask.

After dicing the wafers, the top and bottom parts of the varactor are assembled using thermosonic bonding on a purpose built aligner-bonder. To release the varactor, the top carrier die is removed by dissolving the sacrificial resist in an organic solvent. The solvent is then removed via a freeze drying process. Figure 5 shows a zipping varactor fabricated and assembled using the above surface micromachining process.

4. Measurements

Both shunt- and series-mounted varactors have been fabricated and tested. Two-port measurements were performed on series varactors and one-port measurements were performed on shunt varactors for frequencies ranging from 0.1 to 8.5 GHz. The measured $|S_{21}|$ of this series varactor at different bias voltages is shown in figure 6.

4.1. Equivalent circuit modelling

To extract the capacitance from the measured series varactor, an equivalent circuit model is fitted to the *S*-parameters, as shown in figure 7(*a*). The transmission line elements, Z_L, represent the lossy CPW feed lines between port 1 and reference plane *A* and between port 2 and reference plane *B*. Z_a and Z_e represent the varactor anchor and the bottom electrode, respectively. C_{f1} and C_{f2} are fringe capacitances between the anchor and ground; C_{f3} is the fringe capacitance introduced by the step change in width of the CPW signal line

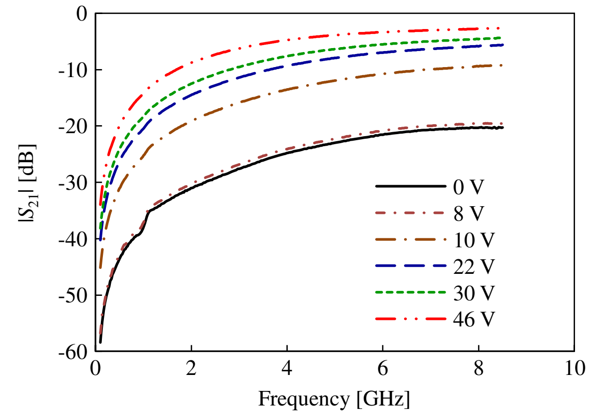

Figure 6. Measured $|S_{21}|$ of a series varactor (including feed lines).

at reference plane *B*; and C_{f4} represents the fringe capacitance between the cantilever anchor and the bottom electrode. Since the dimensions of the varactor (between planes *A* and *B*) are electrically short at frequencies up to 8.5 GHz, the step change in line width has a negligible effect on the varactor performance. L_s is the inductance of the top electrode and the resistances R_s and R_l represent the varactor series resistance and substrate loss, respectively. The parameter-extracted capacitance of the varactor is then obtained from the value of *C*. The value of R_s is 0.1 Ω and R_l is greater than 1 MΩ. L_s is approximately 0.2 nH and the capacitances C_{f1}–C_{f4} are between 3 and 5 fF. Figures 7(*b*) and (*c*) show the magnitude and phase, respectively, of the fitted and measured *S*-parameters at the extreme bias values of 0 and 46 V.

4.2. Measured performance

The parameter-extracted *C–V* characteristic of a series varactor is shown in figure 8. Capacitance values ranging from 20 to 329 fF were measured for bias voltages between 0 and 46 V. When increasing the bias, the varactor exhibits instability at 10 V as the cantilever touches the dielectric. This was predicted in the Coventor model as shown in figure 2 above. However, there is a second unexpected instability in the *C–V* plot between 30 and 32 V, where there is a large increase in capacitance. Although the absolute capacitance ratio of the varactor is 16.5, the varactor demonstrated three distinct stable operating regions. Between 0 and 8 V, the varactor capacitance increases only slightly (20–23 fF) when the cantilever is deflected downwards without contact with the dielectric. Between 10 and 30 V, the capacitance tuning was continuous from 92 to 207 fF. After the second instability, further tuning was possible between 297 and 329 fF. The presence of the tuning instabilities results in hysteresis in the *C–V* characteristic, as indicated by the measurements for decreasing bias.

The bias voltages required for zipping actuation were higher than design values. For this varactor, the area of overlap between the cantilever and the bottom electrode is 380 by 20 μm. In an ideal varactor with perfect contact between the top electrode and the dielectric, the predicted maximum capacitance is approximately 1.17 pF. The capacitance from

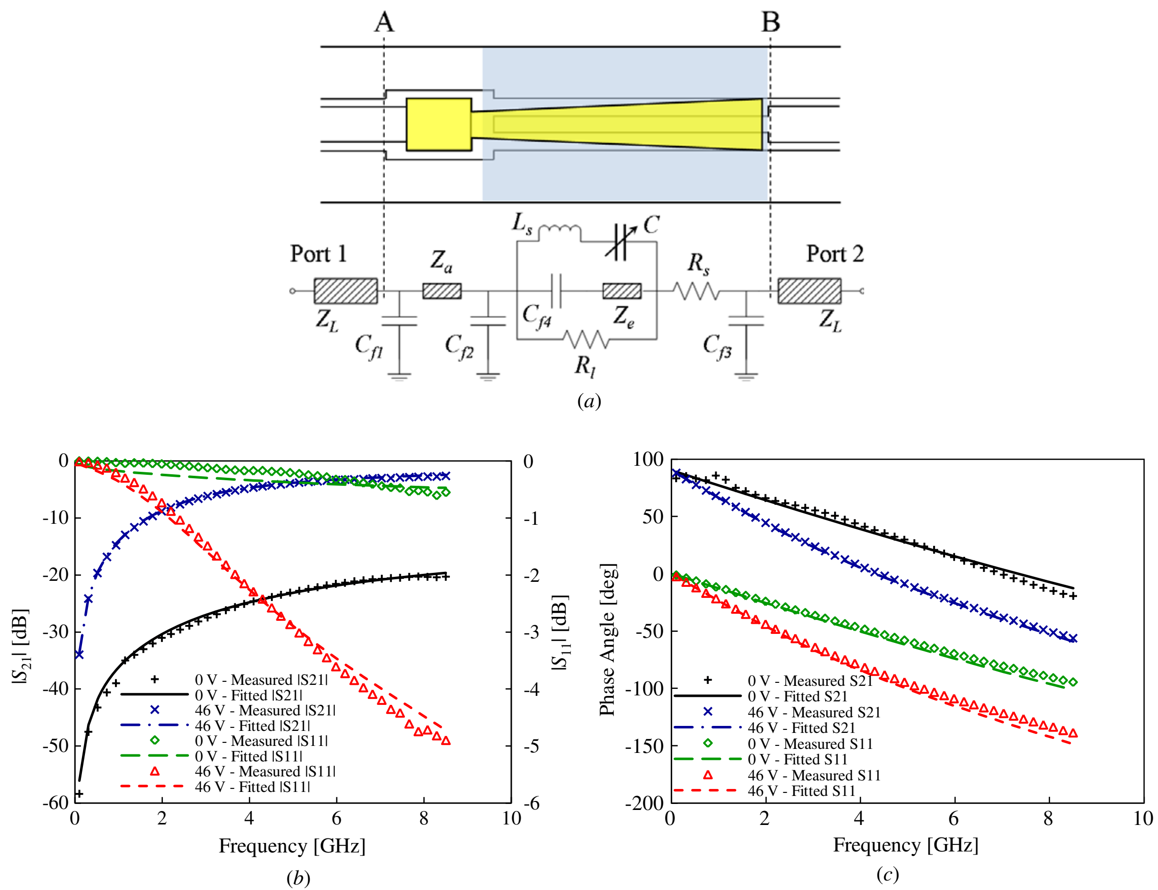

Figure 7. Equivalent circuit model for series varactor: (*a*) schematic layout and equivalent circuit model; (*b*) measured and fitted *S*-parameter magnitude at extreme bias points; (*c*) measured and fitted *S*-parameter phase angle at extreme bias points.

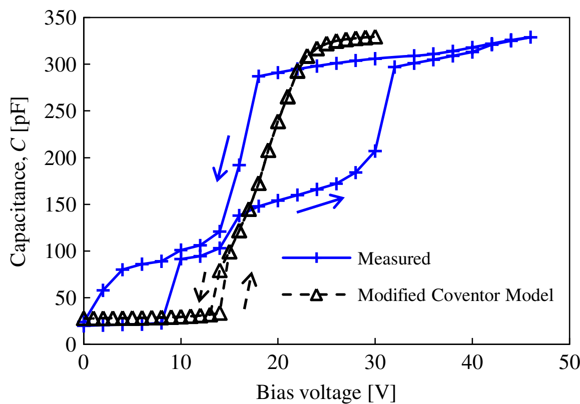

Figure 8. Measured *C*–*V* characteristic against data obtained from a modified Coventor model.

the Coventor model is 1.04 pF at 18 V (see figure 2) since a small air gap is present due to the biaxial curvature of the cantilever. When compared to the model, the measured maximum capacitance is lower by a factor of 3.2. The possible reasons for the discrepancy between model and experimental results are discussed in the next section.

From the equivalent circuit model, the first electrical self-resonant frequency of the series varactor is extrapolated to be 72.6 GHz and 17.2 GHz at 0 V and 46 V bias, respectively. In a measurement for a different zipping varactor, *Q*-factors of 91 (zero bias) and 176 (maximum bias) at 2 GHz were obtained. This varactor is mounted in a shunt configuration and has a length of 300 μm, with a bottom electrode width of 60 μm. Its cantilever width function is $b(x) = 0.36x + 60$ μm, and its minimum and maximum capacitances were 60 and 600 fF, respectively.

5. Discussion

The work reported in this paper represents the first generation of these zipping varactors. The deviation in varactor behaviour from simulation is mainly due to differences in device and model geometry arising from the fabrication process. The high actuation voltages are due to a larger gap in the fabricated device relative to the model. In an ideal zipping varactor, the fixed end of the top electrode should rest on the oxide dielectric at zero bias, i.e. there should be no initial air gap. This would minimize the initial jump (at 10 V in the measured series device) in capacitance and extend the range of stable zipping. Practically, it is difficult to eliminate this gap completely, as a separation δ is required between the anchor and the bottom electrode (see figure 1) and this results in some initial gap. By optimizing parameters such as the initial gap, the curvature of the top electrode and the stiffness of the cantilever, the bias voltage could be reduced.

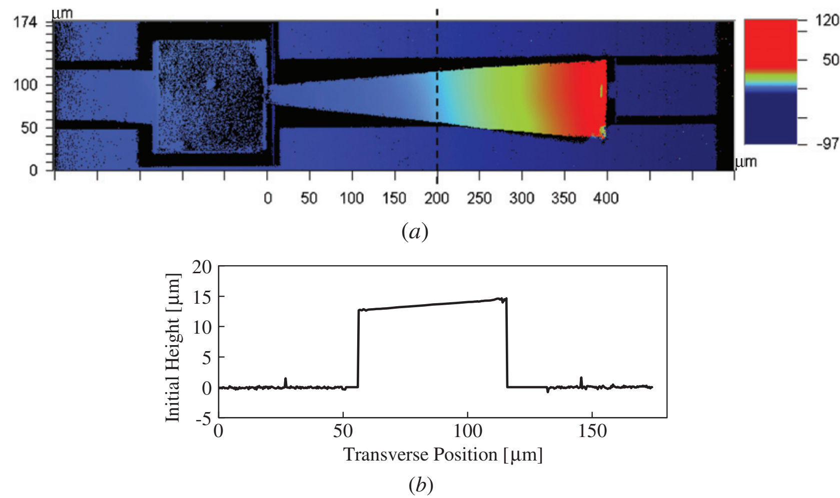

Figure 9. (*a*) Optical interferometric scan of device, and (*b*) profile at mid-span ($x = L/2$).

Figure 9(*a*) shows an optical scan of the series device obtained using a Wyko NT9100 optical interferometer. The profile of the cantilever at its mid-span, plotted in figure 9(*b*), reveals a 1.9° tilt. The cantilever is also off-centre relative to the bottom electrode due to bonding damage in the anchor area. The second unstable jump at 32 V in the measured device could be due to these fabrication imperfections. Further improvements to the fabrication process, such as minimizing over-etching of the seed layer beneath the transmission line and fine tuning the bonding parameters, should improve the assembly process and hence device performance.

The low measured capacitance could be due to a combination of roughness in the oxide and gold, and a lack of planarity in the contact surfaces. In addition, the density of the sputtered SiO_2 dielectric could also be lower than ideal. These factors result in a reduced varactor effective dielectric constant. Figure 10 shows the transverse profile of the oxide surface in a fabricated device in contrast with the flat dielectric surface of the Coventor model (results in figure 2). The transverse curvature of the top electrode (at zero bias) can be approximated using equation (1) above, and this is included in the plot (at an arbitrary height) for comparison. To account for the curvature in the dielectric, the flat dielectric of the model is substituted with a curved dielectric surface, as shown in figure 10. The dielectric curvature of the modified model was chosen such that its average height is the same as that of the actual device. In addition, the dielectric constant of the model varactor is reduced from 4 to 2, to account for surface roughness. Consequently, the maximum capacitance in the model reduces to 0.33 pF, which is close to the measured value. The *C–V* characteristic of the modified model is plotted against the measured data in figure 8.

In order to increase the zipping varactor TR further, a high-permittivity dielectric, such as lead zirconate titanate (PZT), could be integrated into these zipping varactors. The gradual zipping characteristic of the varactor design presented here is suitable for incorporating high-permittivity dielectrics with the potential of realizing a large continuously tunable capacitance range. The varactor could then be made smaller while

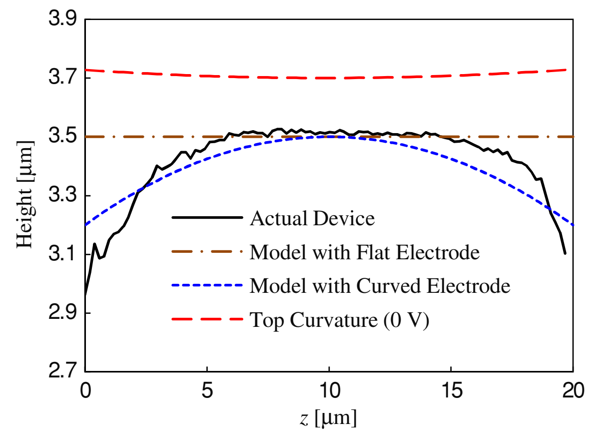

Figure 10. Device and model cross-sectional profiles.

providing larger capacitances. Although the capacitance of a device with a low-permittivity dielectric can be increased by reducing its dielectric thickness, there are practical limitations induced by excessive surface roughness, dielectric breakdown and pinhole defects. Capacitive switches with a high-permittivity dielectric have previously been reported using strontium titanate (STO) [28], and barium strontium titanate (BST) [29, 30]. These switches have superior isolation due to their large on/off capacitance ratios and, for the case of [28], comparable insertion loss to established RF MEMS switches [31]. Typical dielectric loss values for PZT [32] are comparable to those for STO [28] and BST [33] making it suitable as a dielectric material in RF MEMS varactors.

6. Conclusions

RF MEMS zipping varactors with the potential for achieving a large tuning range and high quality factors are reported. These tapered cantilever zipping varactors could be implemented in many tunable microwave applications such as tunable filters, phase shifters, oscillators and reconfigurable antennas. Future work includes optimizing varactor design and fabrication to

obtain improved tuning characteristics. Work is also currently in progress to fabricate zipping varactors with a PZT dielectric.

Acknowledgments

The authors would like to acknowledge helpful discussions with I D Robertson, A J Laister and R E Miles from the University of Leeds. The input from G Dou and M M Ahmad has also been invaluable in the varactor development. This work has been funded by the UK Engineering and Physical Sciences Research Council under the Flagship Project EP/D064805/1 and Platform Grant EP/E063500/1.

References

[1] Lucyszyn S 2004 Review of radio frequency microelectromechanical systems technology *IEE Proc. – Sci. Meas. Technol.* **151** 93–103

[2] Rebeiz G, Entesari K, Reines I, Park S J, El-tanani M, Grichener A and Brown A 2009 Tuning into RF MEMS *IEEE Microw. Mag.* **10** 55–72

[3] Lee C-Y, Chen S-J, Chi D, Yu H and Kim E S 2008 Surface micromachined GHz tunable capacitor with 14:1 continuous tuning range *Proc. IEEE Micro Electro Mechanical Systems (Tucson, AZ, USA, 13–17 January)* pp 1008–11

[4] Rijks T G S M, van Beek J T M, Steeneken P G, Ulenaers M J E, De Coster J and Puers R 2004 RF MEMS tunable capacitors with large tuning ratio *Proc. IEEE Micro Electro Mechanical Systems (Maastricht, Netherlands, 25–29 January)* pp 777–80

[5] Nguyen H D, Hah D, Patterson P R, Chao R, Piyawattanametha W, Lau E K and Wu M C 2004 Angular vertical comb-driven tunable capacitor with high-tuning capabilities *IEEE/ASME J. Microelectromech. Syst.* **13** 406–13

[6] Yoon J-B and Nguyen C T C 2000 A high-Q tunable micromechanical capacitor with movable dielectric for RF applications *Proc IEEE Int. Electron Devices Meeting (San Francisco, CA, USA, 10–13 December)* pp 489–92

[7] Dussopt L and Rebeiz G M 2002 High-Q millimeter-wave MEMS varactors: extended tuning range and discrete-position designs *IEEE MTT-S Int. Microwave Symp. Dig. (Seattle, WA, USA, 2–7 June)* pp 1205–8

[8] Lee H S, Yoon Y J, Choi D-H and Yoon J-B 2008 High-Q, tunable-gap MEMS variable capacitor actuated with an electrically floating plate *Proc. IEEE Micro Electro Mechanical Systems (Tucson, AZ, USA, 13–17 January)* pp 180–3

[9] Yao J J, Park S T and DeNatale J 1998 High tuning-ratio MEMS-based tunable capacitors for RF communications applications *Proc Solid-State Sensor and Actuator Workshop (Hilton Head Island, SC, USA, 8–11 June)* pp 124–7

[10] Young D J and Boser B E 1996 A micromachined variable capacitor for monolithic low-noise VCOs *Proc Solid-State Sensor and Actuator Workshop (Hilton Head Island, SC, USA, 3–6 June)* pp 86–9

[11] Zou J, Liu C, Schutt-Aine J E, Chen J and Kang S-M 2000 Development of a wide tuning range MEMS tunable capacitor for wireless communication systems *Proc. IEEE Int. Electron Devices Meeting (San Francisco, CA, USA, 10–13 December)* pp 403–6

[12] Nieminen H, Ermolov V and Ryhänen T 2001 Microelectromechanical capacitor with wide tuning range *Electron. Lett.* **37** 1451–2

[13] Park J Y, Yee Y J, Nam H J and Bu J U 2001 Micromachined RF MEMS tunable capacitors using piezoelectric actuators *IEEE MTT-S Int. Microwave Symp. Dig. (Phoenix, AZ, USA, 20–25 May)* vol 3 pp 2111–4

[14] Harsh K F, Su B, Zhang W, Bright V M and Lee Y C 2000 The realization and design considerations of a flip-chip integrated MEMS tunable capacitor *Sensors Actuators* A **80** 108–18

[15] Borwick R L III, Stupar P A, DeNatale J F, Anderson R and Erlandson R 2003 Variable MEMS capacitors implemented into RF filter systems *IEEE Trans. Microw. Theory Tech.* **51** 315–9

[16] Hung E S and Senturia S D 1998 Tunable capacitors with programmable capacitance-voltage characteristic *Proc. Solid-State Sensor and Actuator Workshop (Hilton Head Island, SC, USA, 8–11 June)* pp 292–5

[17] Ionis G V, Dec A and Suyama K 2002 A zipper-action differential micro-mechanical tunable capacitor *IEEE Int. Conf. on Micro-Electro-Mechanical Systems* pp 29–32

[18] Nordquist C D, Muyshondt A, Pack M V, Finnegan P S, Dyck C W, Reines I C, Kraus G M, Sloan G R and Sullivan C T 2003 A MEMS high-Q tunable capacitor for reconfigurable microwave integrated circuits *Proc. SPIE* **4981** 1–8

[19] Grichener A, Lakshminarayanan B and Rebeiz G M 2008 High-Q RF MEMS capacitor with digital/analog tuning capabilities *IEEE MTT-S Int. Microwave Symp. Dig. (Atlanta, GA, USA, 15–20 June)* pp 1283–6

[20] Muldavin J, Bozler C, Rabe S and Keast C 2004 Large tuning range analog and multi-bit MEMS varactors *IEEE MTT-S Int. Microwave Symp. Dig. (Fort Worth, TX, USA, 6–11 June)* vol 3 pp 1919–22

[21] Goldsmith C L, Malczewski A, Yao Z, Chen S, Ehmke J and Hinzel D H 1999 RF MEMS variable capacitors for tunable filters *Int. J. RF Microw. Comput.-Aided Eng.* **9** 362–74

[22] Nagano T, Nishigaki M, Kawakubo T and Itaya K 2008 Stable multi-step capacitance control with binary voltage operation at±3V in integrated piezoelectric RF MEMS tunable capacitors *IEEE MTT-S Int. Microwave Symp. Dig. (Atlanta, GA, USA, 15–20 June)* pp 25–8

[23] Pu S H, Holmes A S and Yeatman E M 2007 Design and simulation of zipping variable capacitors *Micro Mechanics Europe (Guimarães, Portugal, 16–18 September 2007)* pp 147–50

[24] Pu S H, Laister A, Holmes A, Yeatman E, Miles R, Robertson I and Dou G 2008 High-Q continuously tunable zipping varactors with large tuning range *Proc. Asia-Pacific Microwave Conf. (Hong Kong and Macau, China, 16–20 December 2008)* pp 1–4

[25] Bozler C, Drangmeister R, Duffy S, Gouker M, Knecht J, Kushner L, Parr R, Rabe S and Travis L 2000 MEMS microswitch arrays for reconfigurable distributed microwave components *IEEE MTT-S Int. Microwave Symp. Dig. (Boston, MA, USA, 11–16 June 2000)* vol 1 pp 153–6

[26] Gray G D, Morgan M J and Kohl P A 2003 Electrostatic actuators and tunable micro capacitors/switches with expanded tuning range due to intrinsic stress gradients *Proc. SPIE* **4981** 202–13

[27] Gray G D, Morgan M J and Kohl P A 2004 Electrostatic actuators with expanded tuning range due to biaxial intrinsic stress gradients *IEEE/ASME J. Microelectromech. Syst.* **13** 51–62

[28] Park J Y, Kim G H, Chung K W and Bu J U 2000 Fully integrated micromachined capacitive switches for RF applications *IEEE MTT-S Int. Microwave Symp. Dig. (Boston, MA, USA, 11–16 June)* vol 1 pp 283–6

[29] Liu Y, Taylor T R, Speck J S and York R A 2002 High-isolation BST-MEMS switches *IEEE MTT-S Int. Microwave Symp. Dig. (Seattle, WA, USA, 2–7 June)* vol 1 pp 227–30

[30] Wang G, Polley T, Hunt A and Papapolymerou J 2005 A high performance tunable RF MEMS switch using barium strontium titanate (BST) dielectrics for reconfigurable antennas and phased arrays *IEEE Antennas Wirel. Propag. Lett.* **4** 217–20

[31] Yao Z J, Chen S, Eshelman S, Denniston D and Goldsmith C 1999 Micromachined low-loss microwave switches *IEEE/ASME J. Microelectromech. Syst.* **8** 129–34

[32] Muralt P 2000 Ferroelectric thin films for micro-sensors and actuators: a review *J. Micromech. Microeng.* **10** 136–46

[33] Setter N *et al* 2006 Ferroelectric thin films: review of materials, properties, and applications *J. Appl. Phys.* **100** 051606(1–46)